Bachelor thesis

Numerical simulations of neutron scattering cross sections for heavy nuclei

Kevin-Alexander Blasl

Supervisor: Assoc.-Prof. Dr. Peter Puschnig*

University of Graz
Institute of Physics

June 12, 2018

*Institute of Physics, Karl-Franzens-Universität Graz, Austria

Abstract

Throughout many experiments in modern day physics one encounters scattering processes for the investigation of material properties, the search for new elementary particles in collision experiments and many other applications. Characterising those experiments is of essential relevance to ensure comparability and one quantity depicting them is the scattering cross section.
In this thesis neutron scattering cross sections for heavy nuclei, described by a Woods-Saxon potential, are being analysed with the aid of numerical simulations using the Numerov method to numerically integrate the radial Schrödinger equation. Furthermore a Python script will be used to compare the dependence of the scattering cross sections on the change of atomic nuclei and neutron energies. Ultimately resonances in the scattering cross sections are being investigated.

Contents

1 Introduction

Scattering experiments are an essential part of today's physical research. They can be performed as a Fix-Target-Experiment or a Collider-Experiment. A very renowned example for a Collider-Experiment is located at the European Organization for Nuclear Research CERN and bears the name ATLAS. The very high relevance of this experiment stems from the experimental proof of nothing less than the Higgs-Boson. In this thesis however, we encounter a Fix-Target-Experiment, consisting of a mono-energetic neutron beam, a film of heavy nuclei and a counter. This kind of experimental setup is often used in material sciences to determine the atomic and molecular structure of solids.

One of many physical quantities resulting from the experiment describing the properties of the solid is the scattering cross section. It gives an information about the probability, that a neutron (or any other particle) is being deflected by a certain angle after the collision with another particle (e.g. a nucleus) and therefore passing a certain area. It depends on the energy of the neutrons and on the atoms that build up the film. These are the parameters that will be varied in the analysis of scattering cross sections at the end of this thesis. The results will give us an insight into the dependence of scattering cross sections on those two parameters and also in eventual resonances.

To round out the discussion about scattering cross sections, the mathematical background will be discussed by describing the experiment in a mathematical way, deriving the scattering cross section from a quantum mechanical point of view and by the depiction of the implementation of the mathematical description in a simulation written in Python.

2 Theory

2.1 Mathematical description of the experiment

To vividly describe scattering processes, one must define certain quantities as well as think about how to describe the parts of the experiment. As our experimental setup consists of neutrons incident on a film of heavy nuclei and a counter, measuring the number of neutrons being scattered to a certain angle, those parts will be a good place to start.
As a natural consequence of the description of quantum mechanics, one does well to describe the incoming free particles as a plane wave $\exp(ikz)$, with z the direction of the momentum vector and $k = \sqrt{2mE}/\hbar$ the wave number. This wave can as well be polarized, but for our description we will neglect the fact of polarization and, as we will see later, therefore not have a dependence on the azimuthal angle ϕ in the function for the outgoing wave.
Further we must consider the heavy nuclei and we will describe them through a potential. The choice of a potential is, however, not arbitrary. As will be discussed later in Subsection 2.2, the choice of the Woods-Saxon potential is a good place to start.
Finally one needs to describe the outgoing particles and because of the choice of plane waves and a potential, one ends up with scattered waves. The mathematical description of the outgoing wave is like the incoming one, however, it can now move in every direction $\vec{r}$ and must decay by $1/r$. Another notable point is the angular dependence, as the neutrons are not uniformly scattered in every direction. That's why one can introduce an amplitude $f(\theta)$, which depends on the polar angle θ but not on the azimuthal angle ϕ as noted earlier. This brings us to the final form for the scattered wave

$$f(\theta)\frac{\exp(ikr)}{r}. \tag{1}$$

Now that we have defined our quantities, we can set them in relation.
In quantum mechanics the central equation for describing any process is the Schrödinger equation

$$-\frac{\hbar^2}{2m}\Delta\psi(\vec{r}) + V(r)\psi(\vec{r}) = E\psi(\vec{r}). \tag{2}$$

There are two more quantities needed to be specified. The mass is represented by the reduced mass of the neutron-nucleus system. The wave function $\psi(\vec{r})$ describes the neutron, so it must be a superposition of the incoming and the outgoing wave in the asymptotic form

$$\psi(\vec{r}) \to \exp(ikz) + f(\theta)\frac{\exp(ikr)}{r}, \qquad r \to \infty. \tag{3}$$

The reason an asymptotic form of the wave function is used, is that the observer (in this case the counter) is far away compared to the size of the neutrons and nuclei and is therefore in the asymptotic region. In this region the incoming wave can be described by a plane wave and the outgoing wave by a spherical wave. [3, p. 229] This fact is implemented by letting $r \to \infty$. This asymptotic form of the wave function describes the neutron beam and its behavior throughout the whole experiment, it is therefore a connection of the mathematical description of the experiment and the physics behind it.
Now we have got all the quantities to solve the Schrödinger equation for the form of $\psi(\vec{r})$.

2.2 Woods-Saxon potential

2.2.1 General information

As mentioned before, the choice of the potential must not be arbitrary and one must consider different types of potentials to find the one suitable for the problem. In our case the Woods-Saxon potential is a very good basis, as it is used to describe the interaction of a neutron with a heavy nucleus, [6, p. 162]. More generally the Woods-Saxon potential is a spherically symmetric potential and describes the forces on each nucleon inside the nucleus in the nuclear shell model. The nuclear shell model assumes that all nucleons form an attractive potential

and each nucleon feels this potential from all the other nucleons. The form of the potential is given by

$$V(r) = -\frac{V_0}{1 + \exp((r - R)/a)}, \tag{4}$$

with V_0 being the potential well depth, a the surface thickness of the nucleus, R the nuclear radius and r the distance to the centre of the nucleus. The minus sign considers the attractive effect of the potential. R is further determined by $R = r_0 A^{1/3}$, with A the mass number of the nuclei and the empirically determined factor $r_0 \approx 1.2fm$. Considering a diffuse potential boundary, this potential can describe the nuclei superior to a simple square well potential. Although this is already an acceptable potential, it can be extended to describe the reality even better.
For instance, the Woods-Saxon potential can be extended by adding an imaginary part to it as well as adding a spin-orbit term. Those two terms will be discussed in the following.

2.2.2 Imaginary part

Extending a potential or any other quantity by an imaginary part is very intuitive, as we must only add an imaginary potential to the real one. This brings us to the form [11]

$$V(r) = -\frac{V_0 + iW_0}{1 + \exp((r - R)/a)}. \tag{5}$$

The main motivation behind introducing an imaginary part into our potential is to consider absorption effects that occur when incoming particles encounter the nucleus. This absorption can be visualised by thinking of it as an absorption of energy. The incident particle encounters the nucleus and in the course of the scattering process it occupies a lower-energy state, whereas the energy difference is almost fully transmitted to the nucleus.

2.2.3 Spin-orbit term

The extension of the Woods-Saxon potential by a spin-orbit term is not so trivial, however, it is highly useful. In the current form the Woods-Saxon potential does not account for *magic numbers* [9]. Those are numbers of neutrons or protons in nuclei which indicate a nucleus with a very high stability in its ground state. *Magic numbers* are e.g. *2, 8, 20, 28, 50, 82, etc.* with their corresponding elements *helium, oxygen, calcium, nickel, etc.* Those nuclei not only have a very high stability compared to neighbouring elements, they do also have a high binding energy as well as a high energy of the first excited state and many other exceptional properties, [2, p. 1679].
The reason it does not describe *magic numbers* correctly, is because it does not consider the spin-orbit interaction, in our case the spin-orbit interaction during scattering processes. It occurs when a particle with spin (in our case a neutron with spin 1/2) is scattered on a barrier in a certain direction. It then makes a difference, whether the orbital angular momentum vector is parallel or anti-parallel to the spin angular momentum vector, as the scattered beams will be diffracted in a slightly different angle. So if an incoming neutron would move on the x-axis and would be scattered and the outgoing beams would lie in the xy-plane, two completely symmetrically arranged counters (in reference to the x-axis, lying in the xy-plane) would measure a different number of diffracted neutrons.
When the spin-orbit term is introduced however, the augmented Woods-Saxon potential does reproduce the correct *magic numbers*.
The spin-orbit term takes the form [9]

$$V_{\mathrm{LS}}(r) = {V_{\mathrm{LS}}}^{(0)} \left(\frac{r_0}{\hbar}\right)^2 \frac{1}{r} \left[\frac{d}{dr} \frac{1}{1 + \exp((r - R)/a)}\right] (\mathbf{L} \cdot \mathbf{S}), \tag{6}$$

with ${V_{\mathrm{LS}}}^{(0)} = 0.44V_0$, $\mathbf{L}$ the *orbital angular momentum of an individual nucleon* and $\mathbf{S}$ the *spin angular-momentum vector.*
The complete form of the Woods-Saxon potential is therefore

$$V(r) = -\frac{V_0 + iW_0}{1 + \exp((r - R)/a)} + {V_{\mathrm{LS}}}^{(0)} \left(\frac{r_0}{\hbar}\right)^2 \frac{1}{r} \left[\frac{d}{dr} \frac{1}{1 + \exp((r - R)/a)}\right] (\mathbf{L} \cdot \mathbf{S}). \tag{7}$$

2.2.4 Python implementation

The calculation of the values of the Woods-Saxon potential on the grid points R for neutrons of energy E, mass number A and atomic number Z is done by the function $v(R, E, A, Z)$, where the potential well depth V_0 is being calculated for all grid points, stored in an array *RR[i]* and passed to the function as the parameter R individually. The parameters given in the associated section are usual literature values, [4, p. 224]. An overflow of the exponential function is being prevented by an if-else condition, that sets the value of the potential equal to zero, as the exponential function is in the denominator of the equation for the potential $V(r)$.

```
# Parameters:
V1     = 56.3    # [MeV]
V2     = 0.32
V3     = 24.0    # [MeV]

a      = 0.75    # surface thickness parameter [fm]
r0     = 1.17    # neutron radius [fm]
expmax = 700.0   # maximum of exponent for exponential function

# Function for the calculation of the Woods-Saxon potential:
def v(R,E,A,Z):
    V0 = V1 - (V2*E) - (V3*(1.0-((2.0*Z)/A)))
    r1 = r0*(A**(1.0/3.0)) # radius of the nucleus
    # Prevention of an overflow:
    if ((R-r1)/a) <= expmax:
        V = -V0 / (1.0+math.exp((R-r1)/a))
    else:
        V = 0.0
    return V
```

2.3 Numerov method

2.3.1 The algorithm

Now that we have mathematically described our experiment and discussed the Woods-Saxon potential, the only piece of the puzzle that is missing, is the Fox-Goodwin method, also called the Numerov method, to numerically integrate the radial Schrödinger equation.
When looking at the Schrödinger equation (2) one can see, that it is a second-order differential equation with a missing first-order derivative term. As this is a very common form of differential equations in physics, there exist various algorithms that can numerically obtain a solution for this equation. The one discussed in the following is called the Numerov method.
To start with the description of the algorithm, we first need to define the quantities we are working with. In our case, the point of interest is the radial part of the Schrödinger equation [4, p. 150]

$$-\frac{\hbar^2}{2m}\frac{d^2}{dr^2}f(r)+\frac{\hbar^2}{2m}\frac{l(l+1)}{r^2}f(r)+V(r)f(r)-Ef(r)=0. \tag{8}$$

In a more compact formulation this takes the form

$$\frac{d^2}{dr^2}f(r)+g(r)f(r)=0, \tag{9}$$

with $g(r)=\frac{2m}{\hbar^2}(E-V(r))-\frac{l(l+1)}{r^2}$. In these two equations l is the angular momentum quantum number and $f(r)$ are the radial functions, which will be treated in greater detail in Subsection 3.1.
The second derivative of $f(r)$ can be rewritten using the result for the central difference derivative for f_i'' [10, p. 21]

$$f_i''=\frac{f_{i+1}-2f_i+f_{i-1}}{h^2}+\mathcal{O}(h^2). \tag{10}$$

This leads to a new form of our compact formulation of the Schrödinger equation

$$\frac{f_{i+1}(r)-2f_i(r)+f_{i-1}(r)}{h^2}+g(r)f(r)=0. \tag{11}$$

This we can rewrite in terms of f_{i+1} as we want to devise an algorithm which computes the next term from previous ones

$$f_{i+1}(r)=2f_i(r)-f_{i-1}(r)-h^2g(r)f(r). \tag{12}$$

To make this equation more accurate one can consider higher order terms. In the result for the central difference derivative higher orders of $\mathcal{O}(h^2)$ appear and we will consider them in our calculations. These terms take the form [10, p. 32]

$$\mathcal{O}(h^2)=-\frac{1}{12}f_{\mathrm{i}}{}^{(4)}(r)h^2. \tag{13}$$

When considering this in equation (10) we get

$$f_{\mathrm{i}}{}''+\frac{1}{12}f_{\mathrm{i}}{}^{(4)}(r)h^2+\mathcal{O}(h^4)=\frac{f_{\mathrm{i+1}}-2f_{\mathrm{i}}+f_{\mathrm{i\text{-}1}}}{h^2}. \tag{14}$$

With equation (9) we get

$$\frac{1}{12}f_{\mathrm{i}}{}^{(4)}(r)h^2+\mathcal{O}(h^4)=g(r)f(r)+\frac{f_{\mathrm{i+1}}-2f_{\mathrm{i}}+f_{\mathrm{i\text{-}1}}}{h^2}. \tag{15}$$

This is the point where the actual Numerov-method comes into play. It uses an operator

$$F:=1+\frac{h^2}{12}\Delta \tag{16}$$

to make the perturbation term of order $\mathcal{O}(h^2)$ disappear and still make use of the central difference derivative, [4, p. 154].
To see the effect of this operator we will apply it to equation (9) and get the following form of the equation

$$\left(1 + \frac{h^2}{12}\frac{d^2}{dr^2}\right)\left[\frac{d^2}{dr^2}f(r) + g(r)f(r)\right] = 0 \tag{17}$$

and from that follows

$$\left(1 + \frac{h^2}{12}\frac{d^2}{dr^2}\right)\frac{d^2}{dr^2}f(r) + g(r)f(r) + \frac{h^2}{12}\frac{d^2}{dr^2}(g(r)f(r)) = 0. \tag{18}$$

Now we can see an important connection to equation (14), where the term $\left(1 + \frac{h^2}{12}\frac{d^2}{dr^2}\right)\frac{d^2}{dr^2}f(r)$ is contained. Reformulating equation (14) for this term and substituting it in equation (18) we get

$$\frac{f_{i+1} - 2f_i + f_{i-1}}{h^2} + \mathcal{O}(h^4) + g(r)f(r) + \frac{h^2}{12}\frac{d^2}{dr^2}(g(r)f(r)) = 0. \tag{19}$$

Terms in $\mathcal{O}(h^4)$ will be neglected for now, as we only want to focus on terms of lower orders. If we now substitute the last term of equation (19) by the central difference derivative of second order, we arrive at the following

$$\frac{f_{i+1} - 2f_i + f_{i-1}}{h^2} + g(r)f(r) + \frac{h^2}{12}\frac{g_{i+1}f_{i+1} - 2f_ig_i + g_{i-1}f_{i-1}}{h^2} = 0, \tag{20}$$

where the h^2 terms cancel out and we can simply solve the equation for $f_{\mathrm{i+1}}$ as we did before

$$f_{\mathrm{i+1}} = \frac{2f_{\mathrm{i}} - f_{\mathrm{i\text{-}1}} - \frac{h^2}{12}(10g(r)f(r) + g_{\mathrm{i\text{-}1}}f_{\mathrm{i\text{-}1}})}{1 + \frac{h^2}{12}g_{\mathrm{i+1}}}.$$

Now we were able to contain the central difference derivative form and get rid of higher order perturbations. The last thing to do is substitute the $f_{\mathrm{i\text{-}1}}, \ldots$ by the correct terms in the sense of grid points. As h is our step size, we denote e.g. $f_{\mathrm{i\text{-}1}} := f(r-h)$ and therefore we get

$$f(r+h) = \frac{2f(r) - f(r-h) - \frac{h^2}{12}(10g(r)f(r) + g(r-h)f(r-h))}{1 + \frac{h^2}{12}g(r+h)}. \tag{21}$$

This equation allows us to now compute every single value on the grid of step size h by knowing the boundary conditions. All we need is a starting point, preferably $f(0)$, and the next point to this one, so $f(0+h)$.

2.3.2 Python implementation

The integration of the radial Schrödinger equation with the Numerov method is being done by a *for-loop*, where the variable $W0$ represents $g(r-h)$, $U0$ represents $f(r-h)$, $W1$ represents $g(r)$, $U1$ represents $f(r)$, $W2$ represents $g(r+h)$ and $U2$ represents equation (21). Using those values the *scattering phase* is being calculated (see equation (32)) and the results are then stored in a list.

```
for l in range(0,lp+1):

    # Initializing values:
    W0 = 0.0
    W1 = ((energy-VV[1])/H2M) - ((l*(l+1))/(HB**2))
    U0 = 0.0
    U1 = 1.0

    # Numerov method:
    for i in range(1,IB):
        W2 = ((energy-VV[i+1])/H2M) - ((l*(l+1))/(RR[i+1]**2))
        U2 = ((2.0*U1)-U0-(((HB**2.0)/12.0) *\
             ((10.0*W1*U1)+(W0*U0)))) / (1+(((HB**2.0)/12.0)*W2))
        W0 = W1
        W1 = W2
        U0 = U1
        U1 = U2

    # Scattering phase:
    A1        = ((B-HB)*sp.spherical_jn(l, (K*(B-HB)))*U1) -\
                (B*sp.spherical_jn(l, (K*B))*U0)
    A2        = ((B-HB)*sp.spherical_yn(l, (K*(B-HB)))*U1) -\
                (B*sp.spherical_yn(l, (K*B))*U0)
    delta[l] = math.atan(A1/A2)
```

3 Derivation of the scattering cross section

3.1 Schrödinger equation and its partial wave expansion and radial functions

An essential part of the derivation of scattering cross sections involves the solution of the Schrödinger equation in spherical coordinates with a spherically symmetric potential, like the Woods-Saxon potential, so that we obtain a wave function with the form shown in equation (3).
First of all, we need to define the scattering cross section. As stated in Chapter 1 it is the probability, that a neutron (or any other particle) is being deflected by a certain angle after the collision with another particle (e.g. a nucleus) and therefore passing a certain area described by the solid angle $d\Omega$. Generally speaking it is the square of the absolute value of the wave function, as this is the probability density for measuring a particle and that's exactly what we aim to achieve. Therefore we can formulate it as

$$\frac{d\sigma}{d\Omega} = |\psi(\vec{r})|^2 = |f(\theta)|^2 \tag{22}$$

where the exponential functions would cancel out because of the complex conjugate of the wave function in the absolute value. To figuratively depict the scattering cross section one can also explain the quantity $d\sigma$ as the cross sectional area spanned by the incoming particles and the quantity $d\Omega$ as the solid angle, those particles are scattered in.
Starting with the Schrödinger equation (2), there are two steps to be done to formulate it in spherical coordinates. First the *Laplacian* has to be formulated in spherical coordinates

$$\Delta = \frac{1}{r^2}\frac{\partial}{\partial r}\left(r^2\frac{\partial}{\partial r}\right) + \frac{1}{r^2\sin(\theta)}\frac{\partial}{\partial\theta}\left(\sin(\theta)\frac{\partial}{\partial\theta}\right) + \frac{1}{r^2\sin^2(\theta)}\frac{\partial^2}{\partial\phi^2} \tag{23}$$

and an ansatz for $\psi(\vec{r})$ has to be made following a *separation ansatz* containing a function only dependent on r and the other one on the angles θ and ϕ

$$\psi(r,\theta,\phi) = R(r)Y(\theta,\phi). \tag{24}$$

A *separation ansatz* is a very common method for solving a *partial differential equation* (PDE), where it is assumed, that the solution of the PDE can be factored into a product form of functions depending on different variables.
Inserting the equations (23) and (24) into the Schrödinger equation (2) we obtain the following equation

$$\begin{aligned} ER(r)Y(\theta,\phi) = \frac{\hbar^2}{2m}\left[\frac{1}{r^2}\frac{\partial}{\partial r}(r^2\frac{\partial}{\partial r}) + \frac{1}{r^2\sin(\theta)}\frac{\partial}{\partial\theta}(\sin(\theta)\frac{\partial}{\partial\theta}) + \frac{1}{r^2\sin^2(\theta)}\frac{\partial^2}{\partial\phi^2}\right] \\ R(r)Y(\theta,\phi) + V(r)R(r)Y(\theta,\phi). \end{aligned} \tag{25}$$

To make use of the *separation ansatz* we can now split the equation in parts only depending on r and parts only depending on θ and ϕ. This brings us to the following form [4, p. 200]

$$\begin{aligned} \frac{1}{R(r)}\frac{\partial}{\partial r}\left(r^2\frac{\partial R(r)}{\partial r}\right) + \frac{2m}{\hbar^2}r^2\left(E - V(r)\right) = \\ -\frac{1}{Y(\theta,\phi)}\left[\frac{1}{\sin(\theta)}\frac{\partial}{\partial\theta}\left(\sin(\theta)\frac{\partial Y(\theta,\phi)}{\partial\theta}\right) + \frac{1}{\sin^2(\theta)}\frac{\partial^2 Y(\theta,\phi)}{\partial\phi^2}\right]. \end{aligned} \tag{26}$$

We can now see that the left hand side only depends on r and the right hand side only depends on θ and ϕ. This is the result we were aiming to get, as we can now set both sides of the equation equal to a constant λ, as both sides depend on different variables and therefore have to be equal to the same constant, leading to

$$\frac{1}{R(r)}\frac{\partial}{\partial r}\left(r^2\frac{\partial R(r)}{\partial r}\right)+\frac{2m}{\hbar^2}r^2\left(E-V(r)\right)=\lambda \tag{27}$$

and

$$-\frac{1}{Y(\theta,\phi)}\left[\frac{1}{\sin(\theta)}\frac{\partial}{\partial\theta}\left(\sin(\theta)\frac{\partial Y(\theta,\phi)}{\partial\theta}\right)+\frac{1}{\sin^2(\theta)}\frac{\partial^2 Y(\theta,\phi)}{\partial\phi^2}\right]=\lambda. \tag{28}$$

The point of interest lies on equation (27) as this is the one that will lead us to the radial Schrödinger equation and finally to the partial wave expansion of the wave function $\psi(\vec{r})$. It depends on the form of the potential, whereas equation (28) stays the same for all spherically symmetric potentials, as it only depends on the angles. To obtain the radial Schrödinger equation it is common to change variables to $u(r)\equiv rR(r)$ and therefore $R(r)\equiv\frac{u(r)}{r}$ and on the other hand reformulate the separation constants to $\lambda=l(l+1)$ with $l=0,1,2,3,\ldots$ [4, p. 200].
When inserting this into equation (27) and executing the partial derivatives as well as reformulating the equation in terms of the simple one-dimensional Schrödinger equation, one obtains

$$-\frac{\hbar^2}{2m}\frac{\partial^2 u_l(r)}{\partial r^2}+\left[V(r)+\frac{\hbar^2}{2m}\frac{l(l+1)}{r^2}\right]u_l(r)=Eu_l(r). \tag{29}$$

This represents the radial Schrödinger equation and compared to the simple one-dimensional Schrödinger equation (2) it is identical to it, with the exception of the potential, which contains a centrifugal part $\frac{\hbar^2}{2m}\frac{l(l+1)}{r^2}$, [7, p. 173]. The solutions of equation (29) are called the *radial functions* $u_l(r)$ with l the *azimuthal quantum number*. The solutions of equation (28) are the *spherical harmonics* $Y_{l,m}(\theta,\phi)$ with m the *magnetic quantum number*, [4, p. 150]. The general solution for the Schrödinger equation can be described by the use of the *spherical harmonics* $Y_{l,m}(\theta,\phi)$ and the radial functions $u_l(r)$ as a superposition of partial waves [4, p. 150]

$$\psi(\vec{r})=\sum_{l,m}\frac{1}{r}u_l(r)c_{l,m}Y_{l,m}(\theta,\phi), \tag{30}$$

with $c_{l,m}$ the expansion coefficients determined by boundary conditions, [4, p. 221].
For all considerations it is essential to keep in mind, that we are looking for scattering solutions with $E>0$ as opposed to bound solutions with $E<0$. To obtain a general form for the wave function in the asymptotic region, we must find radial functions that have an appropriate asymptotic form and that are valid in the interval $[0,\infty]$, therefore also in the asymptotic region. Those radial functions take the form, [4, p. 212]

$$u_l(r)\to a_l\sin\left(kr-l\frac{\pi}{2}+\delta_l\right), \tag{31}$$

with δ_l the *scattering phase*. This quantity describes the process, where the phase of the outgoing wave is shifted with respect to the incoming wave due to the potential of the nucleus. The phase factor is described by $\exp(i\delta_l)$. The equation describing the scattering phase is, [4, p. 211]

$$\delta_l=\arctan\left(\frac{(b-h)j_l(k(b-h))u_l(b)-bj_l(kb)u_l(b-h)}{(b-h)n_l(k(b-h))u_l(b)-bn_l(kb)u_l(b-h)}\right), \tag{32}$$

with k the wave number, j_l the regular and n_l the irregular spherical Bessel functions, b the upper border of the interval $[0,b]$, h the step width, u_l the radial functions and more specific $u_l(b)$ as $f(r)$ and $u_l(b-h)$ as $f(r-h)$ as defined in Subsection 2.3. In this form the scattering phase will also be implemented in the Python program.
Inserting the radial functions into equation (30) we obtain, [4, p. 221]

$$\psi(\vec{r})\to\sum_{l,m}\frac{1}{r}c_{l,m}Y_{l,m}(\theta,\phi)a_l\sin(kr-l\pi/2+\delta_l). \tag{33}$$

3.2 Derivation of the differential and total scattering cross section

To derive the differential and the total scattering cross section we need to find an equation for the scattering amplitude $f(\theta)$, which can be accomplished by expressing the wave functions of equations (3) and (30) in a partial wave expansion and by comparing the coefficients. The trick lies in the origin of equation (31), as it was derived from the partial wave expansion of the wave function (30). This prompts an expansion of the wave function (3) by partial waves and a simple comparison of the new wave function with equation (30). To be specific, equation (3) had the form

$$\psi(\vec{r}) \to \exp(ikz) + f(\theta)\frac{\exp(ikr)}{r}, \qquad r \to \infty$$

so the parts to be expanded by partial waves are $\exp(ikz)$, $\exp(ikr)$ and $f(\theta)$.
Expanding the plane wave in terms of angular coordinates yields, [5, p. 377]

$$\exp(ikz) = \exp(ikr\cos(\theta)) = \sum_{l=0}^{\infty}(2l+1)i^l P_l(\cos\theta)j_l(kr) \tag{34}$$

where the $j_l(kr)$ are the regular spherical Bessel functions, which have an asymptotic form as follows, [4, p. 211]

$$krj_l(kr) \to \sin\left(kr - l\frac{\pi}{2}\right) \tag{35}$$

and can be easily reformulated in terms of exponential functions yielding

$$j_l(kr) \to \frac{1}{2ikr}\left((-i)^l\exp(ikr) - i^l\exp(-ikr)\right). \tag{36}$$

From this we can derive the final form of $\exp(ikz)$, [4, p. 222]

$$\exp(ikz) \to \frac{1}{2ikr}\sum_{l=0}^{\infty}(2l+1)\left(\exp(ikr) - (-1)^l\exp(-ikr)\right)P_l(\cos\theta). \tag{37}$$

This expansion can equally be applied to $\exp(ikr)$.
While the partial wave expansion of a plane wave is well-known, it is not intuitively clear how to expand the amplitude $f(\theta)$. This can be accomplished by expanding it in terms of Legendre polynomials (as the amplitude only depends on the angle θ) with the expansion formula

$$f(x) = \sum_{n=0}^{\infty} b_l P_l(x)$$

where the expansion coefficients are given by

$$b_l = \frac{2n+1}{2}\int_{-1}^{1} f(x)P_l(x)dx.$$

This leads to the expansion of $f(\theta)$ in terms of Legendre polynomials, where the prefactor $(2l+1)/(2ikr)$ has already been separated from the coefficients b_l

$$f(\theta) = \frac{1}{2ik}\sum_{l=0}^{\infty}(2l+1)b_l P_l(\cos\theta), \tag{38}$$

with $P_l(cos(\theta))$ the eigenfunctions to the angular momentum l in form of the Legendre polynomial of order l, [1, p. 209].
Combining the expansions of the plane wave and the spherical wave, we obtain the scattered wave function in the asymptotic area $r \to \infty$

$$\psi(\vec{r}) \to \frac{1}{2ikr}\sum_{l=0}^{\infty}(2l+1)\left[(1+b_l)\exp(ikr) - (-1)^l\exp(-ikr)\right]P_l(\cos\theta). \tag{39}$$

This is the wave function from which we can determine the coefficients b_l by comparison of coefficients. As said before, we compare it to equation (30), more specifically to the solutions of the radial Schrödinger equation and their formulation in terms of exponential functions $u_l(r)$, [4, p. 212]

$$u_l(r) \to a_l \sin\left(kr - \frac{l\pi}{2} + \delta_l\right) = a_l \frac{(-i)^l}{2i} \exp(-i\delta_l) \left[\exp(ikr)\exp(2i\delta_l) - (-1)^l \exp(-ikr)\right]. \tag{40}$$

The terms to be compared are easy to be identified, as we want to obtain the coefficients b_l to be able to fully account for the amplitude $f(\theta)$. It is the first terms in squared brackets and they can directly be compared to each other, as the coefficients a_l can be chosen freely, for they are again a solution of the radial Schrödinger equation according to the superposition principle

$$(1 + b_l)\exp(ikr) = \exp(ikr)\exp(2i\delta_l).$$

Reformulating this in terms of b_l one obtains

$$b_l = \exp(2i\delta_l) - 1. \tag{41}$$

This is a very important point in the derivation of the scattering cross section, as we can now formulate the scattering amplitude $f(\theta)$ by inserting equation (41) into equation (38) yielding

$$f(\theta) = \frac{1}{2ik} \sum_{l=0}^{\infty} (2l+1)(\exp(2i\delta_l) - 1) P_l(\cos\theta), \tag{42}$$

which can be further simplified to

$$f(\theta) = \frac{1}{k} \sum_{l=0}^{\infty} (2l+1)\exp(i\delta_l)\sin(\delta_l) P_l(\cos\theta). \tag{43}$$

According to equation (22), we can finally write the scattering cross section in the following manner:

$$\frac{d\sigma}{d\Omega} = \frac{1}{k^2} \left| \sum_{l=0}^{\infty} (2l+1)\exp(i\delta_l)\sin(\delta_l) P_l(\cos\theta) \right|^2. \tag{44}$$

Equation (44) is sufficient for calculating the scattering cross section, however there is another possible formulation of the scattering amplitude $f(\theta)$, separating it into a real and an imaginary part. This will also be the form we will be using, when implementing it in Python. To derive it, we simply use *Euler's formula* $\exp(iy) = \cos(y) + i\sin(y)$ to obtain

$$f(\theta) = \frac{1}{k} \sum_{l=0}^{\infty} (2l+1) \left(\cos(\delta_l)\sin(\delta_l) + i\sin^2(\delta_l)\right) P_l(\cos\theta) \tag{45}$$

and split it into real and imaginary parts, yielding

$$f(\theta) = \frac{1}{2k} \sum_{l=0}^{\infty} (2l+1)\sin(2\delta_l) P_l(\cos\theta) + \frac{i}{k} \sum_{l=0}^{\infty} (2l+1)\sin^2(\delta_l) P_l(\cos\theta) \tag{46}$$

where the trigonometric identity $\sin(2x) = 2\cos(x)\sin(x)$ has been used. Defining the real part as $g(\theta)$ and the imaginary part as $h(\theta)$

$$g(\theta) := \frac{1}{2k} \sum_{l=0}^{\infty} (2l+1)\sin(2\delta_l) P_l(\cos\theta) \tag{47}$$

$$h(\theta) := \frac{1}{k} \sum_{l=0}^{\infty} (2l+1)\sin^2(\delta_l) P_l(\cos\theta) \tag{48}$$

we arrive at the final form for the differential cross section

$$\frac{d\sigma}{d\Omega} = (g(\theta))^2 + (h(\theta))^2, \tag{49}$$

which will also be the equation used in the Python program computing scattering cross sections.
Now that we have defined the so called differential cross section, there is one more quantity to be specified, called the *total cross section*, which is defined as the integral of the differential scattering cross section over all solid angles. To understand the meaning of the total cross section, one can visualize it as the total cross sectional area of the incoming particle beam scattered by the target (e.g. scattering at a hard sphere gives $\sigma = \pi r^2$, which is just the cross sectional area of the sphere), [7, p. 442].
Now let us bring this into a mathematical form by formulating the integral and solving it

$$\sigma = \int \frac{d\sigma}{d\Omega}(\theta) d\Omega \tag{50}$$

by inserting the differential cross section from equation (44) with $d\Omega = d\phi d(\cos\theta)$ the solid angles. It is very convenient to formulate the differential in θ in terms of $\cos(\theta)$ because the only terms in the differential cross section depending on θ are the Legendre polynomials, which themselves depend on $\cos(\theta)$. This however changes the integral borders to $[-1, 1]$, but leaves the usual integral borders of ϕ as $[0, 2\pi]$ untouched. Inserting this into equation (50) we obtain

$$\sigma = \int_0^{2\pi} d\phi \int_{-1}^{1} \frac{d\sigma}{d\Omega}(\theta) d(\cos\theta) = 2\pi \int_{-1}^{1} \frac{d\sigma}{d\Omega}(\theta) d(\cos\theta).$$

Inserting the differential cross section from equation (44) we obtain

$$\sigma = \frac{2\pi}{k^2} \int_{-1}^{1} \left| \sum_{l=0}^{\infty} (2l+1) \exp(i\delta_l) \sin(\delta_l) P_l(\cos\theta) \right|^2 d(\cos\theta).$$

When performing the square of the absolute values we must not forget about the complex conjugation and we can express the complex conjugated part by using the variable l'. This leads to

$$\sigma = \frac{2\pi}{k^2} \int_{-1}^{1} \sum_{l,l'=0}^{\infty} (2l+1)(2l'+1) \exp(i(\delta_l - \delta_{l'})) \sin(\delta_l) \sin(\delta_{l'}) P_l(\cos\theta) P_{l'}(\cos\theta) d(\cos\theta),$$

where the exponential function now has a minus sign in the exponent due to complex conjugation. Leaving only terms in the integral, that depend on the $\cos(\theta)$ we obtain

$$\sigma = \frac{2\pi}{k^2} \sum_{l,l'=0}^{\infty} (2l+1)(2l'+1) \exp(i(\delta_l - \delta_{l'})) \sin(\delta_l) \sin(\delta_{l'}) \int_{-1}^{1} P_l(\cos\theta) P_{l'}(\cos\theta) d(\cos\theta).$$

The integral may seem hard to solve at first sight, but with a little trick we can obtain the solution using the orthogonality relation of the Legendre polynomials [4, p. 27]

$$\langle L_m | L_n \rangle = \delta_{mn} \frac{2}{2n+1}. \tag{51}$$

This yields

$$\sigma = \frac{2\pi}{k^2} \sum_{l,l'=0}^{\infty} (2l+1)(2l'+1) \exp(i(\delta_l - \delta_{l'})) \sin(\delta_l) \sin(\delta_{l'}) \frac{2}{2l'+1} \delta_{ll'} \tag{52}$$

where the Kronecker delta $\delta_{ll'}$ allows us to simplify equation (52) to

$$\sigma = \frac{4\pi}{k^2} \sum_{l=0}^{\infty} (2l+1) \sin^2(\delta_l), \tag{53}$$

which is the final form for the total cross section.
It is possible to derive the so-called *optical theorem* from this expression, by comparing it to equation (48) to obtain

$$\sigma = \frac{4\pi}{k^2} h(\theta) k \frac{1}{P_l(\cos\theta)} = \frac{4\pi}{k} h(\theta) \frac{1}{P_l(\cos\theta)}$$

and with $\theta = 0$ we obtain the optical theorem, where all $P_l(\cos\theta)$ for $l \geq 0$ are equal to 1

$$\sigma = \frac{4\pi}{k} h(0). \tag{54}$$

3.2.1 Python implementation

With the equations for the differential scattering cross section, the total scattering cross section and the real and imaginary part of the scattering amplitude we can implement this into our Python program to be able to compute scattering cross sections over all solid angles and to see their distribution. It is implemented as follows

```
HPI = math.pi/IPI   # step width on the interval [0, Pi] for theta
for i in range(0,IPI+1):
    theta[i] = i*HPI
    REF      = 0.0
    IMF      = 0.0

    # Calculation of the real and imaginary part
    # of the scattering amplitude:
    for l in range(0,lp+1):
        PLTH  = sp.lpmv(0,l,math.cos(theta[i]))
        REF   = REF + ((0.5/K)*((2.0*l)+1) *\
                ((math.sin(2*delta[l]))*PLTH))
        IMF   = IMF + ((1.0/K)*((2.0*l)+1) *\
                (((math.sin(delta[l]))**2)*PLTH))

    dsigma[i] = (REF**2) + (IMF**2) # diff. sc. cross section

    if i == 0:
        sigma = (((4.0*math.pi)/K)*IMF)*10 # tot. sc. cross section
```

4 Results

In this section all the concepts of the previous chapters are combined to a Python program, which will evaluate differential and total scattering cross sections and detect properties that arise through the variation of the energy and the angular momentum quantum number. The results are then being discussed to obtain information about the nature of scattering. Furhtermore the variation of the stated parameters will make it possible to find resonances. The Python program as well as the formalism we derived in the last chapters is applicable to neutron energies below 50 MeV and elements with mass numbers higher than 40 u, with u the *unified atomic mass unit*. In the periodic table we can start off with the element *Calcium* and end with *Uranium*, as this is the last non-synthetic element that is a solid. As we want a solid target we skip the elements in this range, that are either liquid or gaseous.

4.1 Woods-Saxon potentials

To get a sense of the differences between various nuclei, the Woods-Saxon potentials of the elements *Calcium, Silver* and *Uranium* are plotted in the following. The energy was set to 20 MeV in all three cases to maintain comparability. Furthermore the angular momentum quantum number was chosen as explained in 4.2. The results take the following form:

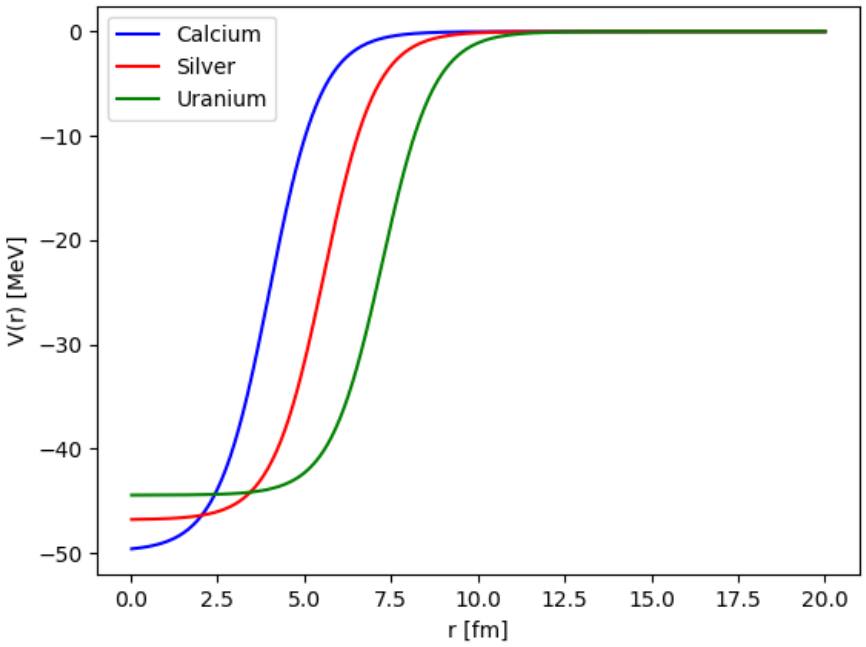

Figure 1: Woods-Saxon potentials for Calcium, Silver and Uranium

As we move from lower to higher mass numbers, we see a change in the potential well depth, whereas lighter elements are described by a deeper potential than heavier elements. In the course of the change in mass numbers, there is also a variation in the range of the potential and it shows, that heavier elements exhibit a longer range. This seems reasonable, as the nuclei of heavy elements contain a higher number of protons and neutrons and are therefore larger in size and energy. Ultimately all three potentials approach a value of 0 MeV in a distance of approximately 10 fm.

4.2 Meaning and influence of the angular momentum quantum number l_p

We will now explain the meaning and influence of the angular momentum quantum number on the differential scattering cross section through results obtained from the Python program.
The angular momentum quantum number l_p is an essential quantity when it comes to scattering processes and can be illustrated easily, when thinking of the scattered particle as a spherical wave, like we did in our theoretical description. In this case l_p constitutes the numbering of partial waves created during the scattering process. The more partial waves we include in the calculation, the more precise the result will become, until we reach a point, where an increase in l_p will not affect the scattering cross section significantly and therefore converge. This l_p constitutes a convergence parameter, which will be useful for all further calculations, as it is a representative value of scattering processes.
So, to find the l_p where the differential scattering cross section does not change anymore, one can evaluate the distribution of differential scattering cross sections for various l_p as will be done in Subsection 4.3 and will find, that this is also the point where the total scattering cross section doesn't change anymore. This can easily be illustrated for the example of the element *Calcium* and a neutron energy of $10MeV$ in the following:

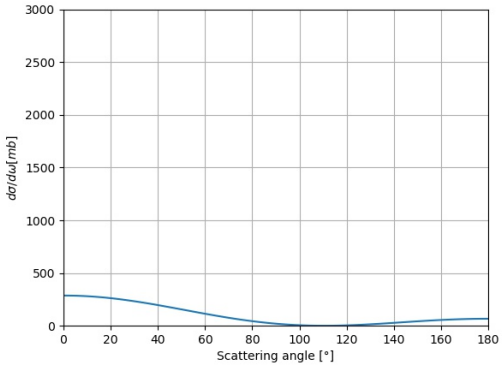

(a) Calcium, E = 10MeV, lp = 1, σ = 909mb

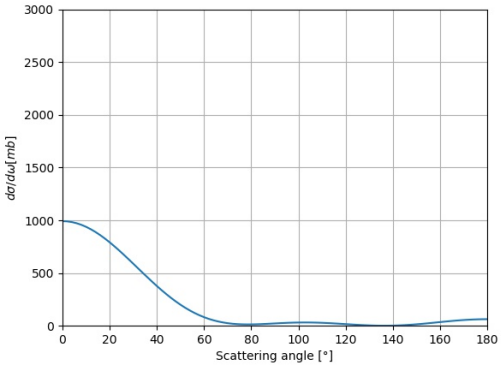

(b) Calcium, E = 10MeV, lp = 2, σ = 1504mb

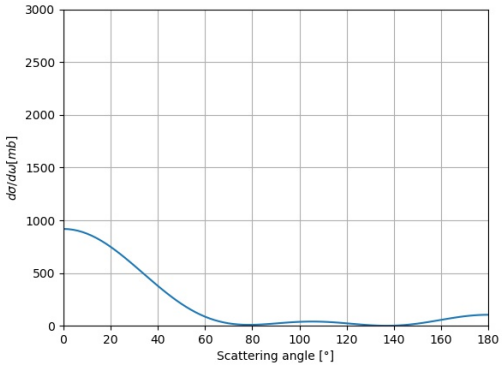

(c) Calcium, E = 10MeV, lp = 3, σ = 1515mb

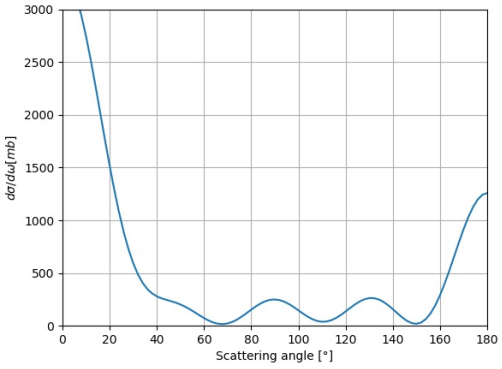

(d) Calcium, E = 10MeV, lp = 4, σ = 3338mb

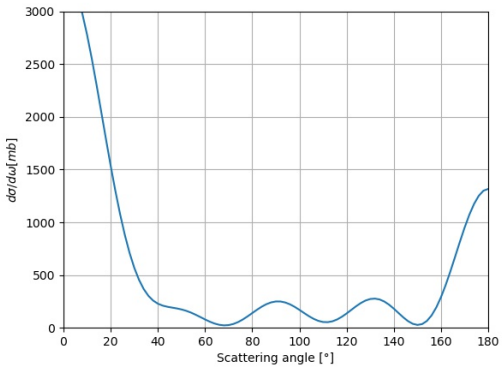

(e) Calcium, E = 10MeV, lp = 5, σ = 3357mb

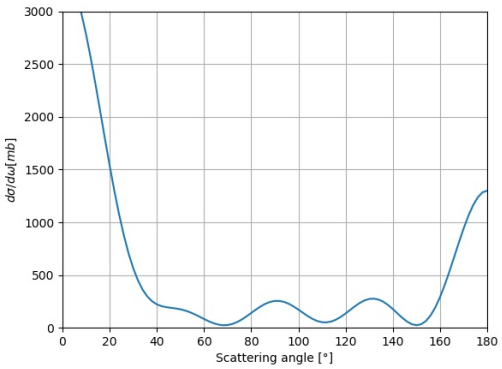

(f) Calcium, E = 10MeV, lp = 6, σ = 3358mb

Figure 2: Differential scattering cross sections for Calcium

Whereas first the value of the total scattering cross section σ increases rapidly, it then slowly approaches $\sigma = 3358mb$ and then stagnates from $l_p = 6$ on. Picturing this is not very representative for Calcium, wherefore the following plot has been made for Uranium. It shows the discussed phenomenon of convergence for energies of $10MeV$ and $50MeV$. Both graphs show the same behaviour, however the maximum l_p for $50MeV$ is higher than for $10MeV$. The fact, that the total scattering cross section is higher for the lower energy, will be discussed in Subsection 4.4.

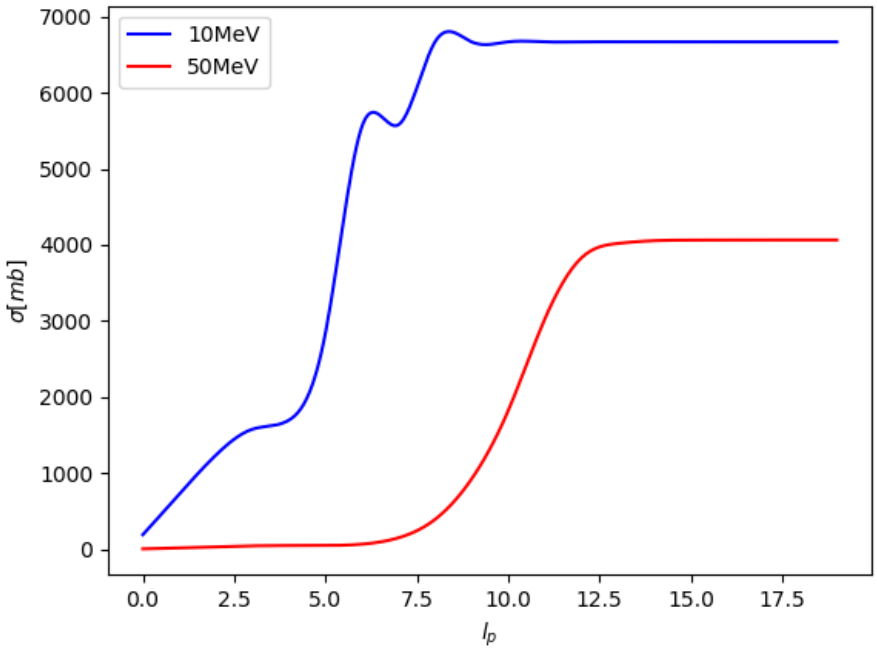

Figure 3: Convergence of l_p for $10MeV$ and $50MeV$

4.3 Scattering cross sections for various elements and their properties

Comparing different distributions of scattering cross sections and analysing their properties and the differences between them, can explain many phenomena that occur during a scattering process.
Differential cross sections for moderately heavy and heavy nuclei are presented with the corresponding energy, angular momentum quantum number and the total scattering cross section. We have checked the convergence of the differential and total cross sections with respect to the maximum angular momentum quantum number in Subsection 4.2 and will use the value the angular momentum quantum number converges towards for each energy for all further calculations.
Moving from moderately heavy to heavy nuclei and likewise from lower to higher energies in the range $[1, 50] MeV$, the scattering cross sections of the elements *Calcium (the lightest), Silver* and *Uranium (the heaviest)* will be analysed. The variation of the energy gives us an insight into the dependence of scattering cross sections on the energy of the incoming particles. Let us put the results for each element in direct comparison and start off with the lightest element, which is Calcium:

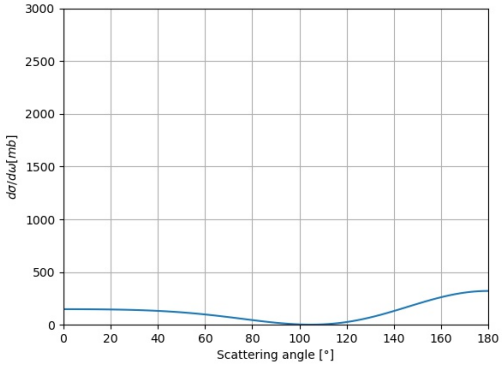

(a) Calcium, E = 1MeV, lp = 2

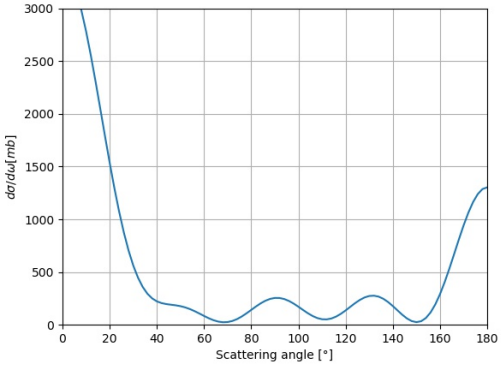

(b) Calcium, E = 10MeV, lp = 6

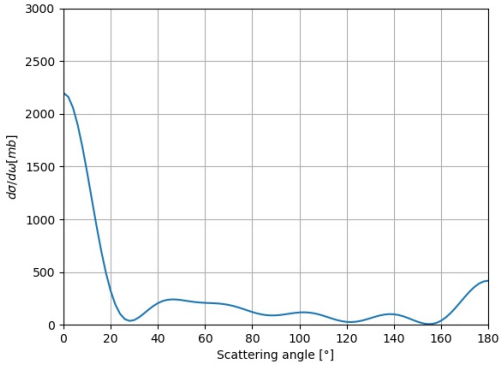

(c) Calcium, E = 20MeV, lp = 8

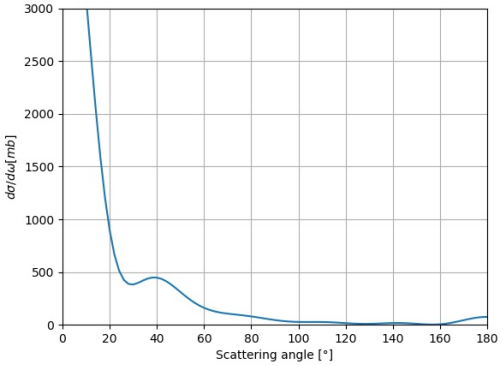

(d) Calcium, E = 30MeV, lp = 9

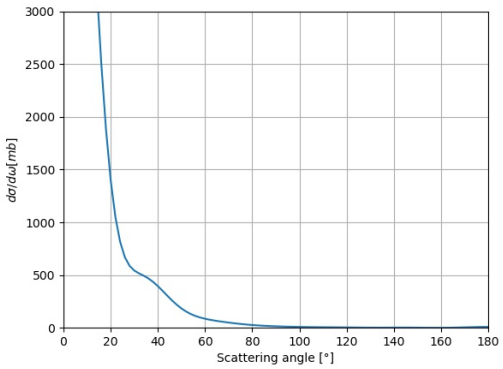

(e) Calcium, E = 40MeV, lp = 11

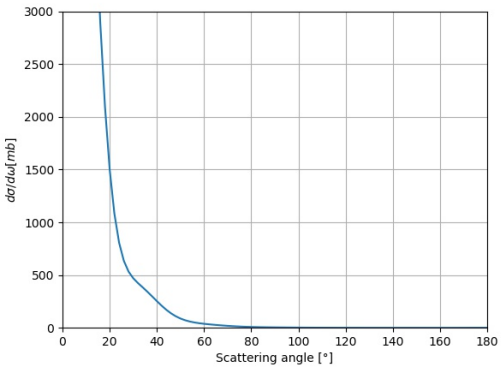

(f) Calcium, E = 50MeV, lp = 13

Figure 4: Differential scattering cross sections for Calcium

When studying these diagrams many interesting properties of scattering processes can be spotted.
In the case of the low neutron-energy of *1 MeV* there is a pretty uniform scattering over all angles. There is, however, a minimum at approximately 105° which tells us, that there is very few to no scattering in this direction. The fact that the differential scattering cross section for about 180° is higher than the one for about 0° tells us, that there are more particles being reflected by the nucleus than there are particles passing the nucleus with a low deflection angle, which seems logical when considering the fact, that the energy is relatively low.
Raising the energy to values of about *10-20 MeV*, first of all the amount of particles passing the nucleus with a low deflection angle increases very strongly, as they have got enough energy to pass it. More interesting however is the fact, that there are more maxima and minima appearing. This finding originates from the properties of the angular momentum quantum number l_p given in Subsection 4.2. The central statement is, that for larger energies increasingly more partial waves need to be considered.
Although more and more partial waves contribute to the scattering cross section the higher the energy is, it is not intuitively discernible from the diagrams. The number of minima and maxima first increases due to more partial waves contributing, however it decreases for higher energies, as the function flattens out and goes to zero for scattering angles of about 60° and higher, because the number of reflected particles goes to zero. This is in good agreement with the intuitive approach, that there will be more particles passing the nucleus with a low deflection angle at high energies. In every energy-step there is a greater number of partial waves contributing, which appears in an increase in the angular momentum quantum number l_p.

We now turn to the results for *Silver*:

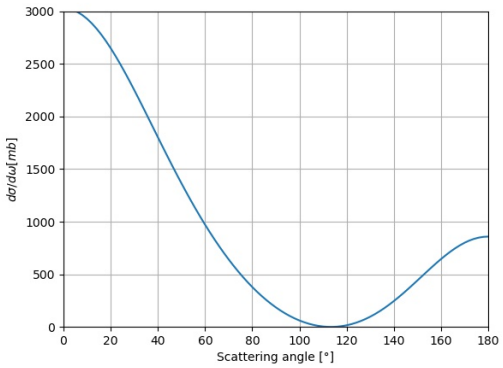

(a) Silver, E = 1MeV, lp = 3

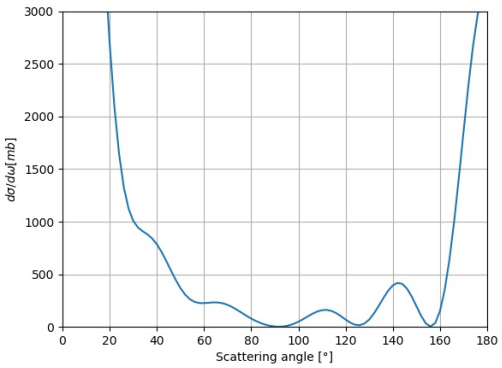

(b) Silver, E = 10MeV, lp = 7

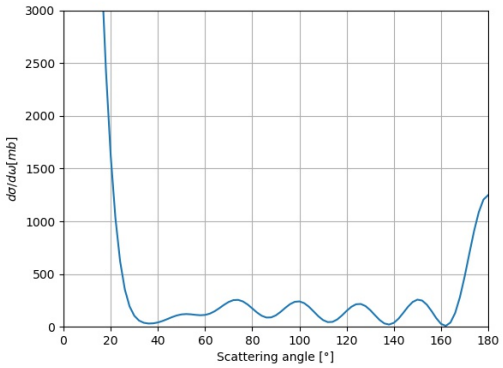

(c) Silver, E = 20MeV, lp = 10

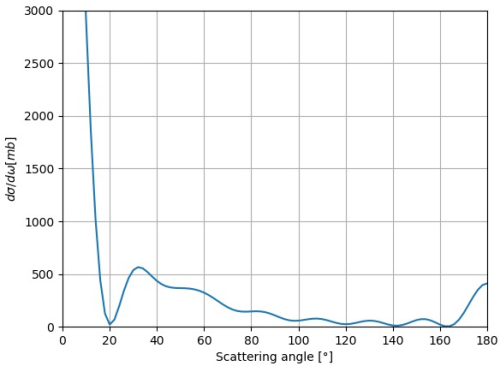

(d) Silver, E = 30MeV, lp = 11

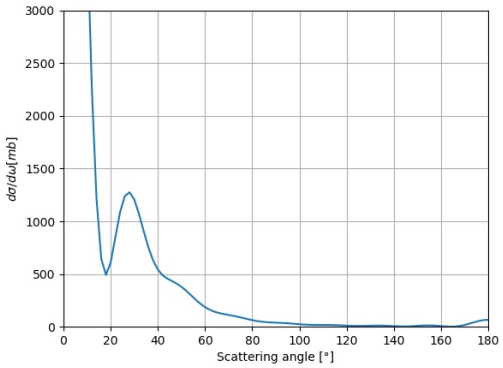

(e) Silver, E = 40MeV, lp = 12

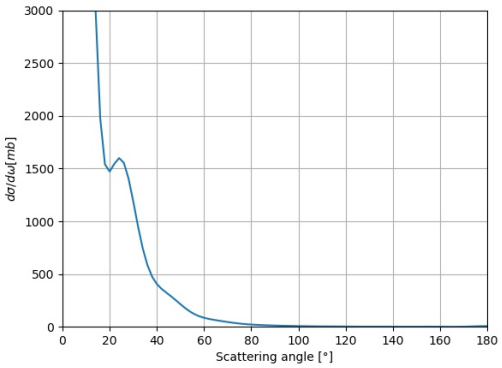

(f) Silver, E = 50MeV, lp = 14

Figure 5: Differential scattering cross sections for Silver

At first appearance one can see a big difference to the distributions of scattering cross sections for Calcium at an energy of $1MeV$. Whereas the scattering to angles of about $0°$ was very low for Calcium atoms, it is extraordinarily high for Silver atoms, although the nucleus is heavier than the one from a Calcium atom.
We will see a contrary behaviour for Uranium again, which is however in agreement with the results for Calcium, which indicates, that Silver takes a special place in this analysis. It can be explained by an observation in Subsection 4.4, where a very strong peak in the resonance energies occurs for low energies. This peak seems rather like a distortion than a

trustworthy value, whereas this phenomenon does indicate a disturbance.
Moving to higher energies we can once more observe the increase in minima and maxima and the following decrease due to the flattening of the distribution. There is, however, a new observation one can make, which is an increase in reflected particles (at about 180° in the diagrams) in comparison to lower-mass nuclei over all energy-steps. This is not surprising, as a higher mass is always connected to a greater amount of reflected particles.
On a final note, one can see the increase in the angular momentum quantum number l_p with the energy once more. This time however, l_p is generally larger than it was for the Calcium atoms.

Now there is only one more element missing, which is *Uranium*:

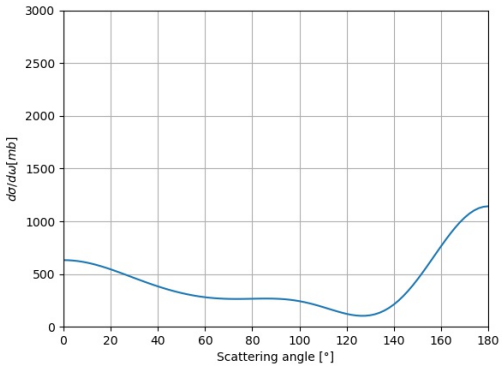

(a) Uranium, E = 1MeV, lp = 3

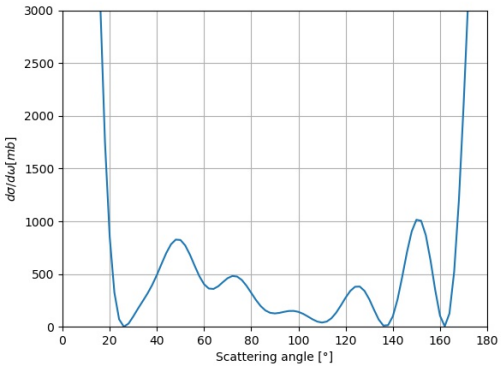

(b) Uranium, E = 10MeV, lp = 8

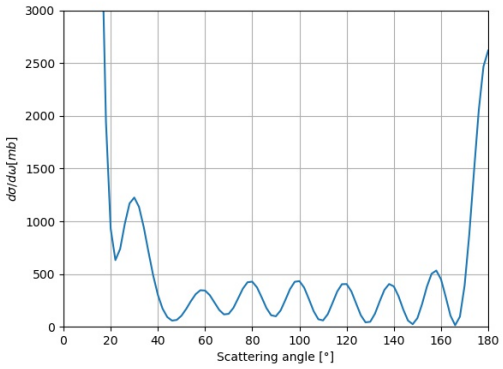

(c) Uranium, E = 20MeV, lp = 11

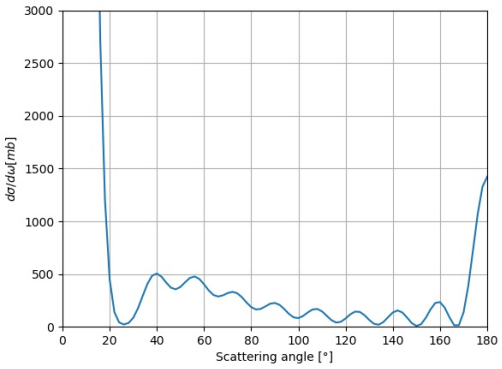

(d) Uranium, E = 30MeV, lp = 14

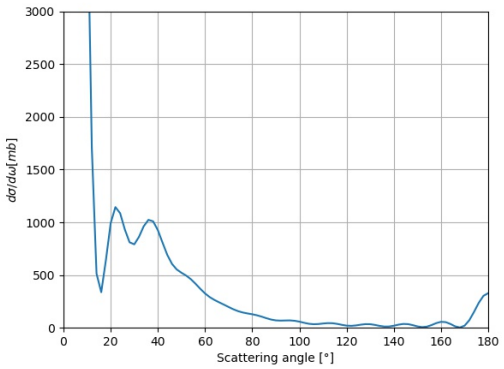

(e) Uranium, E = 40MeV, lp = 15

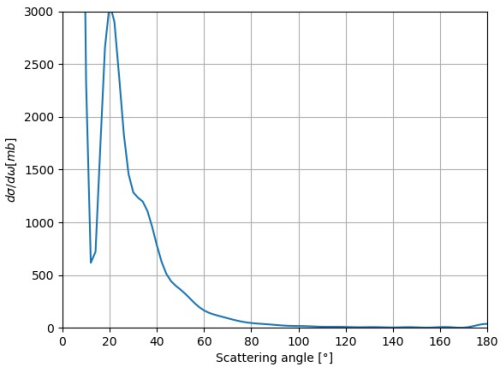

(f) Uranium, E = 50MeV, lp = 16

Figure 6: Differential scattering cross sections for Uranium

An interesting fact to notice here is the decrease of particles passing the nucleus with a low deflection angle at an energy of $1MeV$, although the nucleus is even heavier than for Silver. This fact underpins the view of Silver as an element with a disturbance in the analysis of the behaviour at lower energies.
For energies between $10MeV$ and $30MeV$ there are many particles either being almost completely reflected by the nucleus or passing it with a low deflection angle. The scattering angles in between are sparsely populated. This trend continues for higher energies, whereas the amount of reflected particles decreases as observed for previous nuclei.
As for Uranium it is the element with the most minima and maxima per energy-step, so also with the most partial waves contributing to the scattering cross sections. After we have only mentioned the dependence of partial-wave-contribution on the energy before, we can now be sure about a dependence on the mass of the nucleus as well.
The result for an energy of $50MeV$ has been verified with literature values encountered in [4, p. 229], so the Python program does produce correct results.

4.4 Resonances

There is one last property of scattering processes, that is very vital to many real-life experiments in physics. Especially when searching for new particles this method is highly relevant. It is the search for *resonances* in a scattering process.
Resonances occur, when the number of particles scattered to a certain angle strongly increases for a specific energy. This is the case, when the incident particle and the target form a short-lived semibound state, [8, p. 167].
As we observe the number of particles per energy when looking for resonances, it is equivalent to observing the total scattering cross section per energy. Plotting these two quantities against each other, we can find peaks in the diagram which represent resonances. There can however be several peaks in one diagram, so how can one profoundly distinguish between them?
Finding the answer brings us back to Subsection 4.3 and to plotting differential scattering cross sections against the scattering angle. When doing the same calculations as before, but this time with a resonance energy, one can compare the resulting diagrams and will notice a variation in minima. This is the quantity one can use to characterise resonance energies and it describes the value of the angular orbital momentum. So for a resonance energy, that produces a distribution of differential scattering cross sections with *four* minima, one can say, that it has an orbital angular momentum of $l = 4$, [4, p.230].
Now once more using the Python program, we can calculate the resonance energies for various elements, whereby the angular momentum quantum number l_p is always set to the maximum value explained in Subsection 4.2 for all calculations. Let us analyse the resonance energies for the elements *Calcium, Silver and Uranium* and start off by plotting the total scattering cross section against the energy for a Calcium atom:

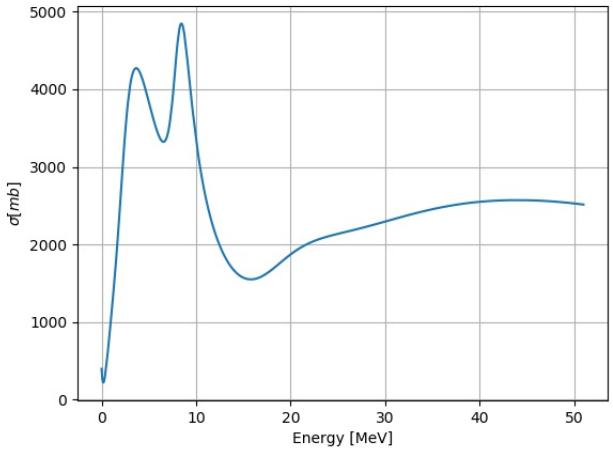

(a) Calcium

Figure 7: Resonance energies for Calcium

There are two peaks visible in the total scattering cross section with values of $\sigma_1 = 4274mb$ and $\sigma_2 = 4849mb$, which are located at the corresponding energies of about $E_1 = 3.657MeV$ and $E_2 = 8.442MeV$. These two values for the energies are our resonances and plotting the distributions of differential scattering cross sections for them will provide the value of the orbital angular momentum of these states.

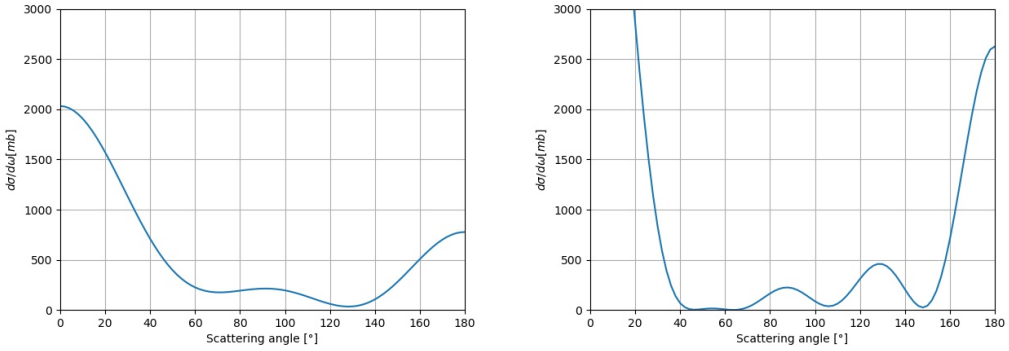

(a) Calcium, $E_1 = 3.657$MeV, $\sigma_1 = 4274$mb, l = 2 (b) Calcium, $E_2 = 8.442$MeV, $\sigma_2 = 4849$mb, l = 4

Figure 8: Differential scattering cross sections for the resonance energies of Calcium

As for the first resonance energy of $E_1 = 3.657$MeV there are two minima, which is connected to a orbital angular momentum of $l = 2$. The second one is related to an orbital angular momentum of $l = 4$.
Continuing this method for Silver and Uranium we obtain the following results:

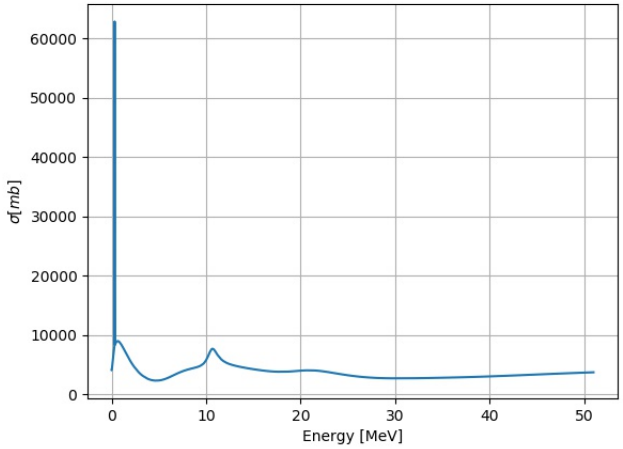

(a) Silver

Figure 9: Resonance energies for Silver

In the case of Silver, there are three peaks, whereas one is very strongly peaked with $\sigma_1 = 62896mb$ at about $E_1 = 0.326MeV$, the second one in the vicinity with $\sigma_2 = 8959mb$ at about $E_2 = 0.647MeV$ and the final peak with $\sigma_3 = 7652mb$ at about $E_3 = 10.688MeV$. As the value of σ_1 is so extraordinarily high and we have observed an unusual behaviour in Subsection 4.3 when analysing the differential scattering cross section at low energies, we will treat this value as a distortion and focus on the other two peaks.
Generating the distributions of scattering cross sections for each we get:

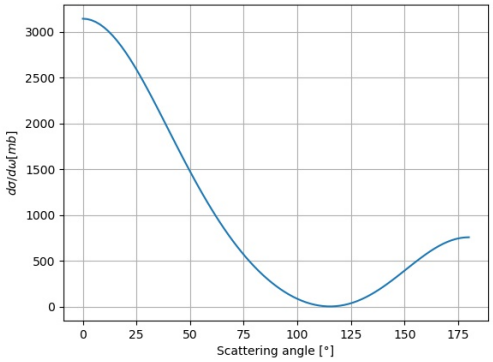

(a) Silver, $E_2 = 0.647$MeV, $\sigma_2 = 8959$mb, l = 1

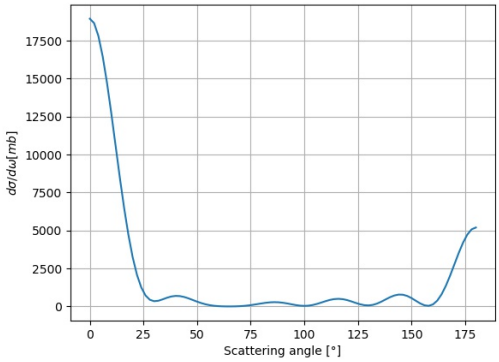

(b) Silver, $E_3 = 10.688$MeV, $\sigma_3 = 7652$mb, l = 5

Figure 10: Differential scattering cross sections for the resonance energies of Silver

Before discussing the results for Silver, let us first generate the results for Uranium and then discuss them collectively. For Uranium we obtain the following results:

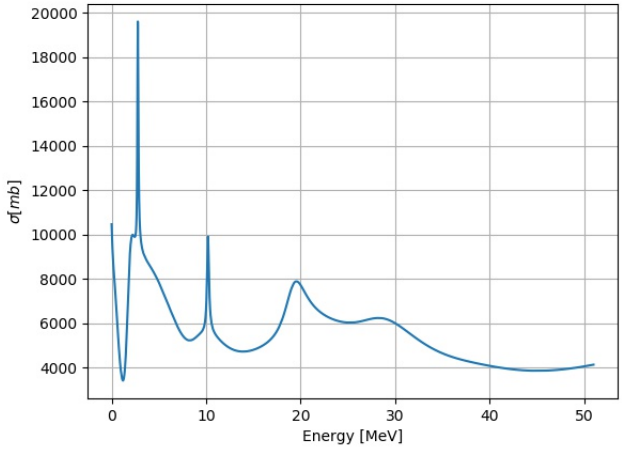

(a) Uranium

Figure 11: Resonance energies for Uranium

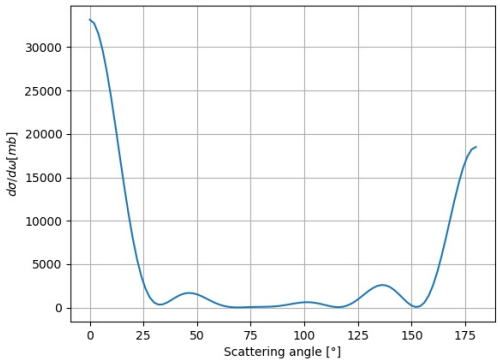

(a) Uranium, $E_1 = 2.778$MeV, $\sigma_1 = 19615$mb, l = 4

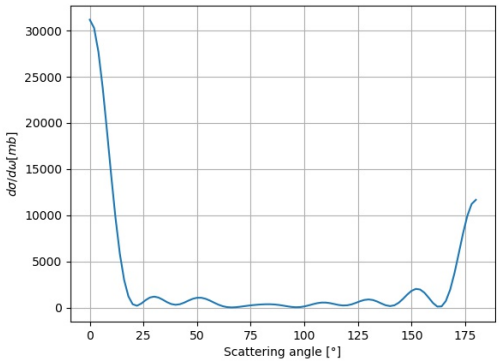

(b) Uranium, $E_2 = 10.2$MeV, $\sigma_2 = 9918$mb, l = 7

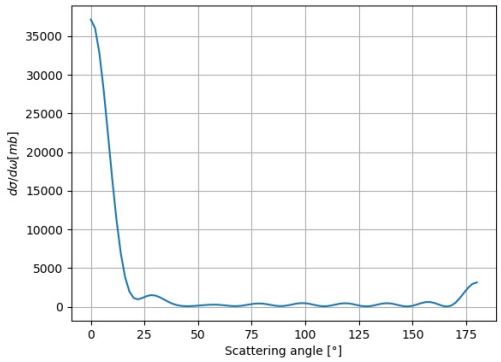

(c) Uranium, $E_3 = 19.56$MeV, $\sigma_3 = 7898$mb, l = 8

Figure 12: Differential scattering cross sections for the resonance energies of Uranium

Comparing the number of resonance energies for all three nuclei they stay to a greater or lesser extent the same for all cases, so we can not state a significant dependence on the mass number. However, there is an observable increase in the number of minima and therefore the orbital angular momentum, connected to an increase in energy. This stands in good agreement with the rise of the angular momentum quantum number l_p associated with the energy.
For all three elements, even for the heaviest non-synthetic element Uranium, the resonances lie in a range of $0MeV < E_{res} < 20MeV$, so the higher energies are pretty much excluded from resonances and show the common behaviour of a consistent decrease. This seems reasonable when thinking about what happens during the scattering process. When the incident particle hits the target with a high energy, the speed connected to this energy will be too big and the time that the particle stays in the immediate vicinity of the target too low, as they could form a semibound state. So the energy must not be arbitrary as to form a bond between the particle and the target, which is represented in the results.

5 Summary

In this thesis, the main concepts of describing scattering processes were discussed. Besides a mathematical description of the experiment, also the characterisation of the scattering nucleus has been made through a Woods-Saxon potential and its general properties were discussed. We have learned, that a Woods-Saxon potential describes the nucleus superior to a simple square-well potential and that it can be extended by both an imaginary part for describing absorption processes and a spin-orbit term for describing the effects of spin-orbit interaction. Following this, the Numerov method for integrating the radial Schrödinger equation was presented and explained in detail.
With the learned methods the radial Schrödinger equation and both the differential and total scattering cross section were derived. From the derivation we have already learned some essential properties of scattering processes, such as the existence of a scattering amplitude and a scattering phase causing a phase shift on the outgoing wave.
Writing a Python program computing the differential as well as the total scattering cross section using the learned methods and extending it by the property of calculating resonances, which are short-lived semibound states of the incident particle and the target, we then generated diagrams and results for target nuclei formed by the elements *Calcium, Silver* and *Uranium* and compared them to each other.
The results were in good agreement with an intuitive approach to scattering, whereby the reflection of particles decreases with an increase in energy. Furthermore, we observed an increase in the angular momentum quantum number, describing partial waves contributing to the scattering, when increasing the energy of the incident particles or the atomic mass of the nucleus. Once more both results stand in good agreement with today's theoretical description of scattering and also with the intuitive idea, that higher energies can generate a higher amount of partial waves during a scattering process.
Finally, resonances were observed for each of the three elements and we found a slight increase in resonance energies that accompanies an increase in the mass number. However, this can not be stated generally, as with only a slight increase it was not significant.
The methods presented in this thesis can be used to numerically calculate both differential and total scattering cross sections for moderately heavy to heavy atoms for energies of $0 < E \leq 50MeV$, which was implemented in the Python program which can plot the results as well as find resonances in various setups.

List of Figures

References

[1] Christoph Scholz Bogdan Povh, Klaus Rith. *Teilchen und Kerne: Eine Einführung in die physikalischen Konzepte*. Springer-Verlag, 1993.

[2] Robert Resnick David Halliday. *Physik, Teil 2*. Walter de Gruyter, 1994.

[3] Fritz Ehlotzky. *Quantenmechanik und ihre Anwendungen*. Springer, 2006.

[4] W. Loesch Erich W. Schmid, G. Spitz. *Theoretische Physik mit dem Personal-Computer*. Springer-Verlag, 1987.

[5] Torsten Fliessbach and Hans Walliser. *Arbeitsbuch zur Theoretischen Physik, 2. Auflage*. Spektrum - Akademischer Verlag, 2008.

[6] Siegfried Fluegge. *Practical Quantum Mechanics*. Springer, 1974.

[7] David J. Griffiths. *Quantenmechanik*. Pearson, 2012.

[8] Robert Mann. *An Introduction to Particle Physics and the Standard Model*. CRC Press, 2010.

[9] S.A. Alavi M.R. Pahlavani. Solutions of Woods–Saxon Potential with Spin-Orbit and Centrifugal Terms through Nikiforov–Uvarov Method. *Communications in Theoretical Physics*, 58(5):739–743, 2012.

[10] Peter Puschnig. Computerorientierte Physik PHY.J10, WS 2017/18, January 2018. URL: `http://physik.uni-graz.at/~pep/CompOriPhys/CoP2017.pdf`. Last visited on 2018/06/09.

[11] Erich Vogt. The thickness of the nuclear surface. *Physics Letters*, 1(3):84–87, 1962.